Spectrum of classical two-dimensional Coulomb clusters

K. Nelissen,[1,*] A. Matulis,[1,2,†] B. Partoens,[1,‡] M. Kong,[1,3] and F. M. Peeters[1,§]
[1]*Departement Fysica, Universiteit Antwerpen, Groenenborgerlaan 171, B-2020 Antwerpen, Belgium*
[2]*Semiconductor Physics Institute, Goštauto 11, LT-01108 Vilnius, Lithuania*
[3]*Institute of Plasma Physics, Chinese Academy of Sciences, Hefei, Anhui, 230031, China*
(Received 22 June 2005; published 17 January 2006)

The frequency spectrum of a system of classical charged particles interacting through a Coulomb repulsive potential and which are confined in a two-dimensional parabolic trap is studied. It is shown that, apart from the well-known center-of-mass and breathing modes, which are independent of the number of particles in the cluster, there are more "universal" modes whose frequencies depend only slightly on the number of particles. To understand these modes the spectrum of excitations as a function of the number of particles is compared with the spectrum obtained in the hydrodynamic approach. The modes are classified according to their averaged vorticity and it is shown that these "universal" modes have the smallest vorticity and follow the hydrodynamic behavior.

DOI: 10.1103/PhysRevE.73.016607 PACS number(s): 45.20.−d, 45.05.+x

I. INTRODUCTION

Classical clusters of repulsive particles confined in traps have been both theoretically and experimentally a study object for many decades due to their applicability to a wide variety of systems. Recently, there has been considerable theoretical and experimental progress in the study of mesoscopic systems consisting of a finite number of charged particles confined in a parabolic trap. These systems are composed of a finite number of charged classical particles which can move in a two-dimensional (2D) plane and are confined in the plane by an external applied potential. They are the classical analog of the 2D quantum dot. Typical experimental realizations of such systems are electrons on the surface of liquid helium [1], electrons in quantum dots [2], plasmas with dust particles [3], ion traps [4], vortices in superfluids [5], confined ferromagnetic particles [6], charged metallic balls above a plane conductor [7], and colloidal crystals [6,8]. The 2D charged clusters also resemble the problem of charge distribution studied by Mayer [9] and by Thomson in his "plum-pudding" model of the atom [10,11].

Such Coulomb clusters with a finite number of particles (typical $N<100$) have been extensively studied during the past few years. Theoretically the configurations [12,13], the transitions to metastable states [13,14], normal modes [15], and the melting properties have been studied.

Recently, also experimentally the dynamical properties of Coulomb clusters have been studied in which a selective excitation of modes was performed [16,17]. The successful extraction of the excitation spectrum from the thermal Brownian motion of the particles in the cluster [18] apparently shows the usefulness of such 2D finite Coulomb clusters with a small number of particles being an ideal tool for comparison with detailed modeling.

Motivated by the experimental ability of selectively excitation of modes, we performed a detailed study of the spectrum of a Coulomb cluster, traced the dependence of the modes on the number of particles, and compared the spectrum with the hydrodynamic treatment.

The paper is organized as follows: in Sec. II we present our simulation method for the discrete system and in Sec. III we present the hydrodynamic approach. In Sec. IV the results of both models are compared, and the vorticities of the different modes are calculated. In Sec. V our conclusions are formulated.

II. DISCRETE SYSTEM SIMULATION

We consider the classical 2D system consisting of charged particles which are laterally confined by a parabolic potential and interact through the Coulomb potential. The system is described by the Hamiltonian

$$H=\frac{1}{2}m^*\omega_0^2\sum_{i=1}^{N}r_i^2+\frac{1}{\epsilon}\sum_{i<j}^{N}\frac{e^2}{|\mathbf{r}_i-\mathbf{r}_j|}, \tag{1}$$

where m^* is the effective mass of the particle, ω_0 is the confinement frequency, and ϵ is the dielectric constant of the medium where the particles are moving in. If we choose $r_0=(e^2/\epsilon m^*\omega_0^2)^{1/3}$ as the length unit and $E_0=m^*\omega_0^2r_0^2$ as the energy unit [19–25], the Hamiltonian can be expressed in dimensionless form as

$$H=\frac{1}{2}\sum_{i=1}^{N}r_i^2+\sum_{i<j}^{N}\frac{1}{|\mathbf{r}_i-\mathbf{r}_j|}. \tag{2}$$

To find the minimum energy configuration we used the Monte Carlo simulation technique extended with a Newton optimization technique, as first used in Ref. [15]. In order to be sure to have found the ground state configuration, one has to run the Monte Carlo simulation routine many times starting with a different initial random configuration. The spectrum of all system excitations and the corresponding particle

*Electronic address: kwinten.nelissen@ua.ac.be
†Electronic address: amatulis@takas.lt
‡Electronic address: bart.partoens@ua.ac.be
§Electronic address: francois.peeters@ua.ac.be

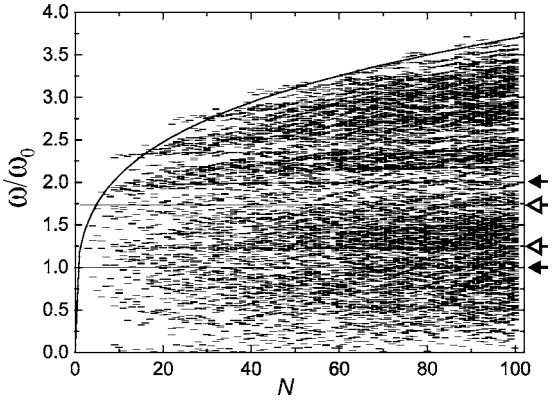

FIG. 1. Excitation spectrum (the frequency is in units of ω_0).

velocities for every excitation mode were defined via the diagonalization of the dynamical matrix, which is given by

$$\frac{\partial H}{\partial r_{\alpha,i}\partial r_{\beta,j}}, \tag{3}$$

with α and $\beta=x,y$ and i,j denoting the particle number.

To be sure that the obtained configuration is a stable one, the lowest eigenvalue of the dynamical matrix is checked to be positive.

The obtained excitation spectrum for clusters containing up to $N=100$ particles is shown in Fig. 1. The solid curve approximately indicates the upper limit of this spectrum. The two frequencies which are independent of the number of particles are clearly seen: the center-of-mass mode with $\omega=1$ and the breathing mode with $\omega=\sqrt{3}$, indicated by the black arrows. However, a close inspection reveals that more horizontal lines are present; some of them are indicated by the open arrows in Fig. 1. The existence of such modes whose frequency is almost independent of the number of particles is better seen in the frequency histogram shown in Fig. 2. The histogram was calculated taking into account the frequencies

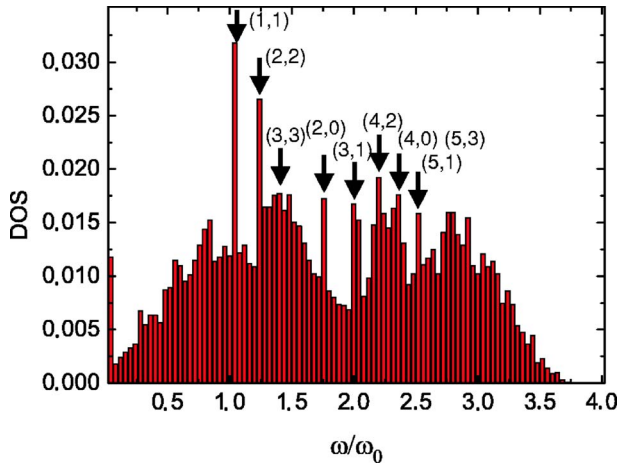

FIG. 2. (Color online). Density of states (DOS) obtained by using an averaging over intervals with $\Delta\omega/\omega_0=0.04$. Clusters are considered with particles from $N=2$ to $N=200$. The arrows mark the states which coincide with the hydrodynamic model labelled with the integer numbers (j,m).

for all systems with different numbers of particles ranging from 2 to 100. Peaks in Fig. 2 indicate that in the considered system there are excitation modes with a frequency which almost does not depend on the number of particles in the cluster. As shown in the next section, they are related to the excitation frequencies in the hydrodynamic approach where all frequencies are independent of the number of particles.

III. HYDRODYNAMIC APPROACH

The hydrodynamic approach for 2D dots in a perpendicular magnetic field for various circular confinements was developed in Ref. [27]. As shown in the Appendix, the global, static properties of the cluster, like the cluster energy and its radius, as obtained with the hydrodynamic model agree rather well with the results obtained from the simulations for the discrete model. This motivated us to compare also the dynamical properties like the frequency spectrum for both models. The hydrodynamic model is based on the solution of the Laplace equation for the potential created by the electrons. Spheroidal coordinates are used with boundary conditions ensuring a constant chemical potential inside the dot.

The solution leads to the static electron density (in r_0^{-2} units)

$$\rho_0 = \frac{3N}{2\pi R^2}\sqrt{1-r^2/R^2}, \tag{4}$$

and the chemical potential

$$\mu = R^2, \tag{5}$$

where

$$R = (3\pi N/4)^{1/3} \tag{6}$$

is the hydrodynamic dot radius in our scaled variables.

The excitations of the system are described by the linearized continuity equation for small density deviations $\rho(t)$ from the equilibrium density distribution and for the particle velocities $\mathbf{v}(t)$, the equation of motion in the simplest Drude approximation, and the Laplace equation for potential deviation $\phi(t)$ with the corresponding boundary conditions, namely,

$$\frac{\partial}{\partial t}\rho + \nabla(\rho_0\mathbf{v}) = \mathbf{0}, \tag{7a}$$

$$\frac{d}{dt}\mathbf{v} = \nabla\phi, \tag{7b}$$

$$\nabla^2\phi = \mathbf{0}, \tag{7c}$$

$$\left.\frac{\partial\phi}{\partial z}\right|_{\substack{z=0\\ r<R}} = 2\pi\rho. \tag{7d}$$

According to the scaling used the time is measured in ω_0^{-1} units and the velocity in $r_0\omega_0^{-1}$ units. Additionally, charge conservation is assumed.

Assuming the usual exponential time dependence $\exp(-i\omega t)$ of all small deviations $[\rho(t)$, $\phi(t)$, and $\mathbf{v}(t)]$ we

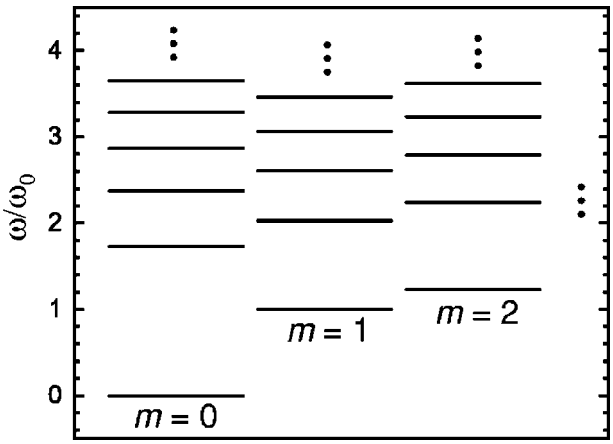

FIG. 3. Excitation spectrum as obtained from the hydrodynamic approach for different m values.

arrive at a time-independent set of equations. According to the solution presented in Ref. [27], this problem is diagonalized in spheroidal coordinates. The electron density in the dot [in polar coordinates $\mathbf{r}=(r,\theta)$] for a specific excitation mode is given by the expression

$$\rho(\tau,\theta)=\frac{1}{\tau}P_j^{|m|}(\tau)e^{im\theta},\quad \tau=\sqrt{1-r^2/R^2}, \tag{8}$$

and the corresponding frequency reads

$$\omega_{jm}^2=\frac{4}{\pi L_j^{|m|}}\{j(j+1)-m^2\}. \tag{9}$$

Here the symbol $P_j^m(x)$ stands for the Legendre polynomial of the first kind, and

$$L_j^{|m|}=2\frac{\Gamma\left(\frac{j+|m|}{2}+1\right)\Gamma\left(\frac{j-|m|}{2}+1\right)}{\Gamma\left(\frac{j+|m|+1}{2}\right)\Gamma\left(\frac{j-|m|+1}{2}\right)}, \tag{10}$$

where $\Gamma(x)$ is the gamma function. All modes are marked by two integers: the non-negative number j and the orbital number m, which gives the number of nodes in the orbital part of the density. The difference between these numbers is even. Thus, one can write $j=|m|+2k$, where the non-negative integer radial number k actually gives the number of density nodes along the radius.

In the asymptotic region of large m and k values, a more simple expression for the frequencies can be obtained. Replacing the gamma functions in Eq. (10) by their Stirling asymptotic expression one can easily obtain that in this region the frequencies are given by

$$\omega_{jk}^2\approx\frac{4}{\pi}\sqrt{j^2-m^2}\approx\frac{8}{\pi}\sqrt{k|m|}. \tag{11}$$

The spectrum of the cluster excitations as it is given by Eq. (9) is shown in Fig. 3.

In contrast to the averaged properties of the cluster, which coincide for the discrete and the hydrodynamic models rather well (see the Appendix), the more detailed characteristics of the dot are much more sensitive to the choice of the model. One of those sensitive characteristics is the spectrum of excitations, and as seen from first sight the spectrum obtained by the numerical simulation of the discrete system (Fig. 1) and the one obtained from the continuous hydrodynamic model (Fig. 3) differ very much.

Comparing these two spectra we notice two essential differences. First, the spectrum in the hydrodynamic approach extends up to infinity while the frequencies of the discrete model are confined to a restricted frequency interval. Next, the spectrum of the hydrodynamic model has a gap $(0<\omega<1)$ where there are no excitation levels at all, while in the case of the discrete model this gap is filled with levels (see Fig. 1).

The physical origin of the first discrepancy is evident. The excitations with large frequencies correspond to large m and k numbers, or a large number of azimuthal and radial nodes in the mode density function of expression (8). They cannot all be realized in the discrete model due to the finite number (N) of electrons and as a consequence there are only $2N$ eigenmodes. Assuming an equidistant location of particles in the dot, we can estimate the number of radial nodes as $k\approx\sqrt{N/12}$ and the number of azimuthal nodes as $m\approx\sqrt{3N/16}$. Inserting these expressions into Eq. (11), which is valid for large frequency values, we obtain an estimation for the maximum frequency

$$\omega_{\lim}\sim N^{1/4}. \tag{12}$$

Thus, only in the region $\omega\ll\omega_{\lim}$ can one expect a coincidence of the hydrodynamic spectra and the one from the discrete model.

Note that the upper frequency limit for the discrete model (see the solid curve in Fig. 1) was obtained numerically by fitting the above expression, giving

$$\omega_{\lim}=1.17N^{1/4}. \tag{13}$$

The second difference, the gap in the hydrodynamic spectrum, has also a clear physical reason. Due to the finite dimensions of the dot, the actual wavelengths of excitations are limited from above, what leads to a frequency limitation from below. Moreover, in the hydrodynamic model the electrons are considered as a charged liquid which does not resist shear deformations. Consequently, various types of rotating excitations are possible, and all of them have zero frequency. Mathematically this fact follows from Eq. (7). Namely, there are numerous solutions of the aforementioned equation set with $\rho(t)=\phi(t)=0$ and the excitation velocity obeying the equation

$$\boldsymbol{\nabla}(\rho_0\mathbf{v})=\mathbf{0}, \tag{14}$$

which are excitations with zero current divergence. Thus, in the hydrodynamic approach the zero level frequency is multiple degenerate and contains all rotating modes. On the other hand, it is easy to check [it follows from Eq. (7b)] that all other hydrodynamic modes (with $\omega\neq 0$) obey the condition

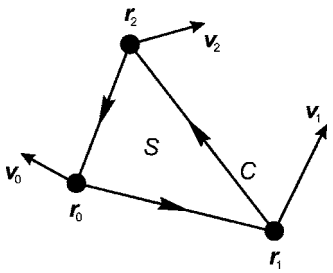

FIG. 4. The definition of the approximate local vorticity.

$$\mathrm{rot}\mathbf{v} = \mathbf{0}, \tag{15}$$

or equivalently have zero vorticity.

In the discrete model (where all electrons are arranged into a finite size Wigner crystal) there is a resistance to shear deformations. Thus, the aforementioned hydrodynamic zero frequency level is split and redistributed over the complete frequency range. This leads to the idea to classify the modes in the discrete model according to their vorticity. Only the modes with small vorticity can be expected to be close to their hydrodynamic analogs.

IV. VORTICITY

In the discrete model the local vorticity can be defined approximately using the triangle composed of an electron at point $\mathbf{r}_0$ and its two closest neighbors (at points $\mathbf{r}_1$ and $\mathbf{r}_2$) as depicted in Fig. 4. We define the local vorticity as the following integral of the rotor of the velocity over the above triangle area:

$$\gamma(\mathbf{r}_0) = \frac{1}{S}\int d^2r(\mathrm{rot}\mathbf{v})_z = \frac{1}{S}\oint_C d\mathbf{r}\mathbf{v}$$

$$\approx \frac{1}{2S}(\mathbf{v}_2\mathbf{r}_1 + \mathbf{v}_3\mathbf{r}_2 + \mathbf{v}_1\mathbf{r}_3 - \mathbf{v}_1\mathbf{r}_2 - \mathbf{v}_2\mathbf{r}_3 - \mathbf{v}_3\mathbf{r}_1). \tag{16}$$

We define a global vorticity for a specific mode as the absolute value of the above local vorticity averaged over all electrons.

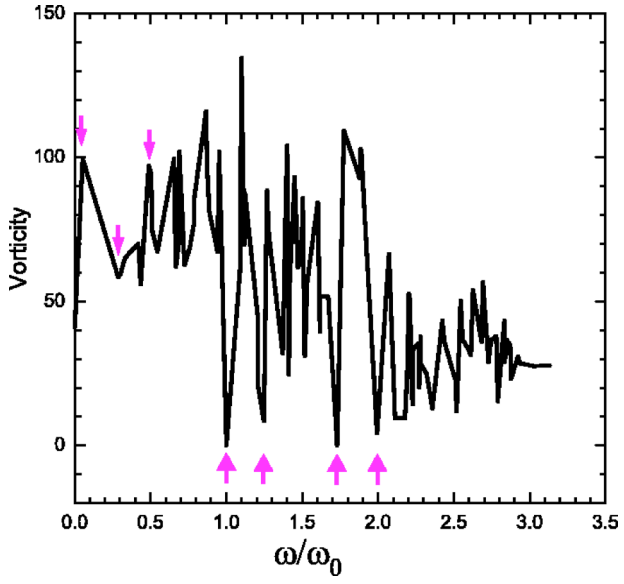

FIG. 5. (Color online). The vorticity of all modes for $N=50$.

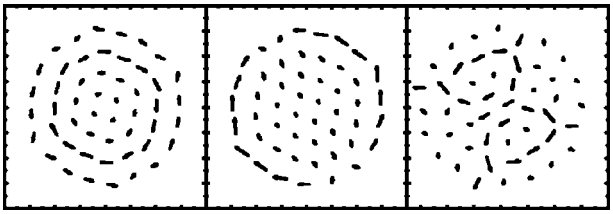

FIG. 6. Velocity distribution for the modes indicated by the three small arrows in Fig. 5 in the $0<\omega<1$ frequency gap for an $N=50$ system, corresponding to the downward arrows in Fig. 5.

As an example, the above global vorticity is shown in Fig. 5 for an $N=50$ particle cluster as a function of frequency. The vorticities for clusters with different numbers of particles are similar. It is remarkable that there is an evident gap in the region $0<\omega<1$ with large vorticity. In this region there are no modes with small vorticity, which agrees with our earlier assertion that these modes are originating from the degenerate zero frequency level of rotating modes of the hydrodynamic model. Some of these rotating modes are shown in Fig. 6 and correspond with the downward arrows in the vorticity plot of Fig. 5. In the region $\omega>1$ the modes with a rather small vorticity are clearly seen. Four of them indicated by arrows are the same modes that are marked in Figs. 1 and 5. One may expect that the frequencies of these modes have to be rather close to the ones obtained in the hydrodynamic model. To confirm this statement we present in Fig. 7 the frequency of the modes from the discrete model with the smallest vorticity (black circles on the plot) and compare them with the lowest frequencies obtained in the hydrodynamic model which are indicated by the horizontal lines. We see that with increasing number of electrons the frequencies from the discrete model and those from the hydrodynamic model start to coincide. This was further confirmed by the close similarity of the electron velocity distribution for both models which are shown in Fig. 8. In the first two columns the velocities of the discrete model are presented for a 50- and a 150-particle system, respectively, and in the third column is the velocity distribution of the hydro-

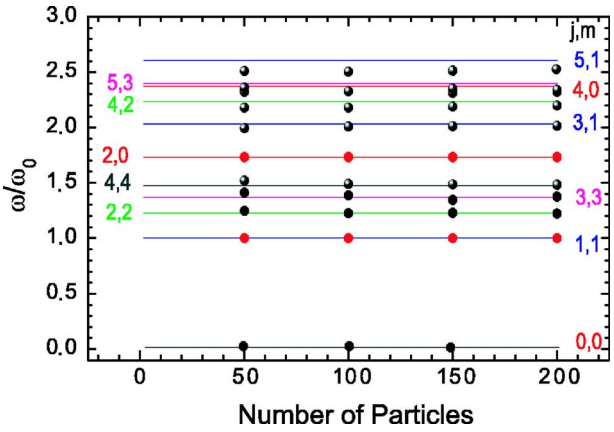

FIG. 7. (Color online). Comparison of the frequencies of the hydrodynamic model (horizontal lines) and the low vorticity modes of the discrete model (dots) as a function of the number of particles.

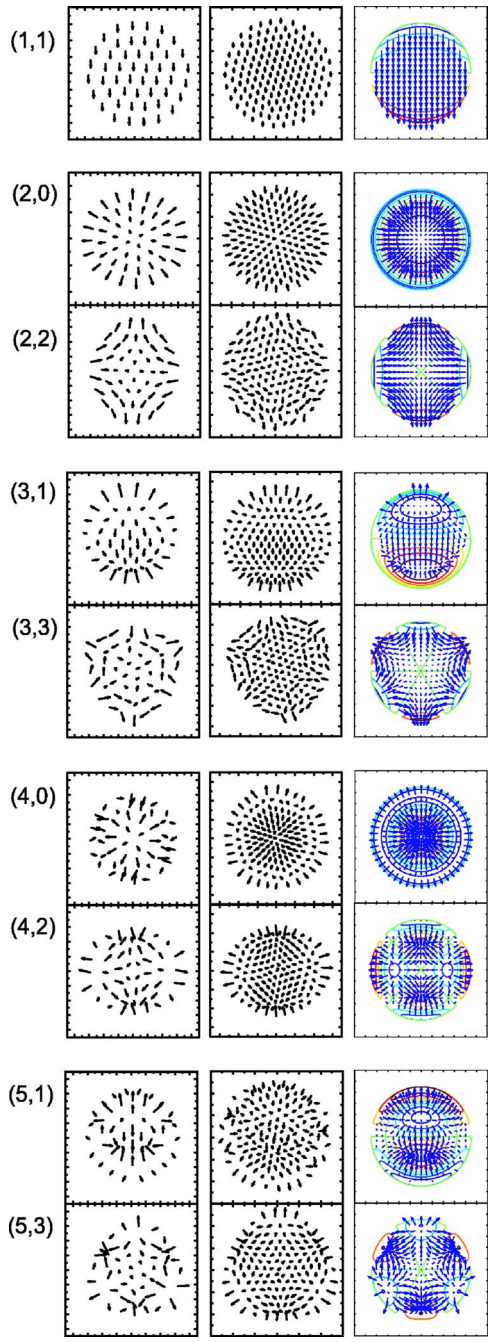

FIG. 8. (Color online). Velocity distribution for the coinciding modes in the discrete and the hydrodynamic models. In the first two columns the velocities of a 50- and 150-particle system are presented, respectively. These results are compared in the third column with the one from the hydrodynamic model. The contour plot in the third column shows the density of particles.

dynamic model. This velocity distributions can be useful to extract these modes from future experimental data. In Figs. 7 and 8, and in Fig. 2 as well, the hydrodynamic modes are indicated by two integers $\{j,m\}$. Thus, we showed clearly that the low vorticity frequencies in the spectrum of the discrete model tend very slowly to the hydrodynamic analog when the number of particles is incremented.

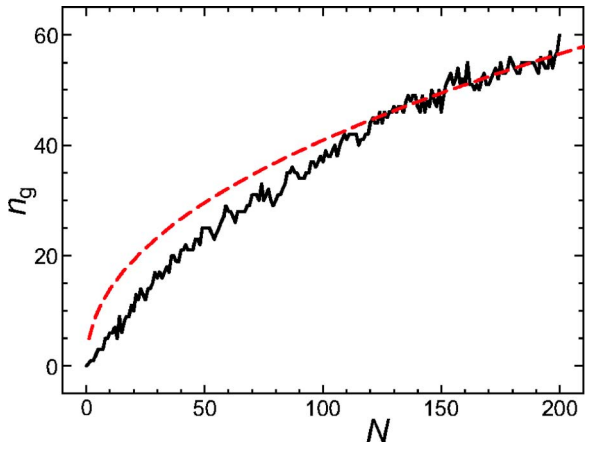

FIG. 9. (Color online). Number of modes in the $0<\omega<1$ frequency gap as a function of the number of particles. The dashed curve shows the $N\to\infty$ asymptotic behavior.

The last question which we still have to answer is the behavior of the modes in the discrete model in the frequency gap. For this purpose we counted the number n_g of those modes in the $0<\omega<1$ region. Its dependence on the number of particles in the cluster is shown in Fig. 9. The dashed curve shows the asymptotic behavior of this quantity for a large number of particles in the cluster. The latter was obtained by fitting the calculated data using a logarithmic scale in the region $N=120-200$, and the expression of this curve reads

$$n_g \approx 4.7N^{0.47}. \tag{17}$$

Thus, the number of modes in the gap increases with the number of particles. Nevertheless, as the total number of modes increases as $2N$, the relative number of modes in the frequency gap is

$$n_g/2N \approx 2.3N^{-0.53} \to 0 \tag{18}$$

and decreases. Moreover, the averaged density of modes can be estimated as

$$2N/\omega_{\mathrm{lim}} = 2N/1.17N^{1/4} \sim N^{3/4}, \tag{19}$$

while the density of modes in the frequency gap actually is given by Eq. (17). So, we see that as the number of particles grows, the ratio of the density of modes in the gap to the averaged density tends to zero as well, and, consequently, in this sense the discrete model tends to the hydrodynamic model as well.

V. CONCLUSIONS

In this paper we performed a detailed study of the spectrum of Coulomb clusters, traced its dependence on the number of particles, and compared the results with the hydrodynamic approach. We found out that it is convenient to classify the modes of the discrete model according to their global vorticity.

In the frequency region $0<\omega<1$ only modes with large vorticity are present. They originate from the degenerate hy-

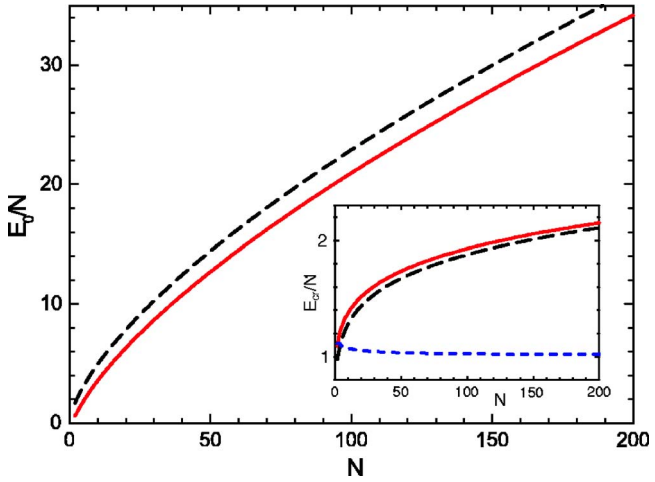

FIG. 10. (Color online). Energy per particle in the cluster: solid curve—discrete model, dashed line—hydrodynamic model Eq. (A1). Inset: solid curve—crystallization energy per particle, dashed curve—Eq. (A3), short dashed curve—the ratio of the above quantities.

drodynamic state corresponding to zero frequency, where all possible rotations of the liquid droplet are included. As the number of particles is incremented the density of modes in this region becomes negligible as compared with the total averaged density in the cluster.

In the region $\omega > 1$ there are modes with a rather small vorticity. As the number of particles in the cluster grows, the frequencies of these modes tend to their analogs in the hydrodynamic model. The velocity distributions of the hydrodynamic model pretty well coincide with the distributions obtained in the discrete model for the above modes with small vorticity and, thus, they may be useful for experimental purposes.

ACKNOWLEDGMENTS

This work was supported by the Flemish Science Foundation (FWO-Vl), the "Belgian Science Policy," the EU network of excellence, SANDiE, and the Flemish-China bilateral program.

APPENDIX: THE ENERGY AND THE RADIUS OF THE CLUSTER

In this appendix we consider the behavior of two global properties of the cluster—the averaged energy per particle E_0/N and the maximum radius of the cluster.

The averaged energy per particle for the discrete model is shown by the solid curve in Fig. 10. The dashed curve shows the same quantity, which was calculated in the hydrodynamic model integrating the chemical potential [see Eq. (5)] over the number of particles in the cluster, namely,

$$E_0(N) = \int_0^N \mu(N')dN' = \left(\frac{3\pi}{4}\right)^{2/3} \int_0^N N'^{2/3} dN' = a_0 N^{5/3}, \tag{A1}$$

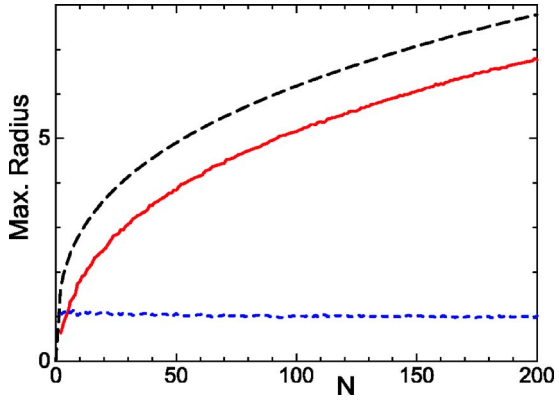

FIG. 11. (Color online). Maximum radius of the cluster: solid curve—discrete model, dashed curve—hydrodynamic model Eq. (6), short dashed curve—the difference between the above quantities.

$$a_0 = \frac{3}{5}\left(\frac{3\pi}{4}\right)^{2/3} \approx 1.06.$$

Thus, in the hydrodynamic approach the energy per particle is $a_0 N^{2/3}$.

In the inset of Fig. 10 the difference between these energies is shown by the solid curve. We see that it increases with the number of particles in the cluster. The physical origin of this discrepancy is the crystallization energy. Following the idea of the local density approximation, it can be estimated by averaging the crystallization energy for the homogeneous crystal over the surface area occupied by the cluster. The crystallization energy per particle for the homogeneous crystal was obtained in Ref. [28], and for the hexagonal lattice it is

$$E_{\rm cr}^{\rm (hom)}/N = c_0\sqrt{\rho}, \quad c_0 \approx 1.96. \tag{A2}$$

Now replacing the homogeneous density in the above equation by the density of the cluster (4) and averaging it over the cluster we obtain the following expression for the average crystallization energy:

$$E_{\rm cr} = c_0 \int_{r\leqslant R} d^2 r \rho_0^{3/2}(r) = \frac{c_0 (3N)^{3/2}}{R\sqrt{2\pi}} \int_0^1 dr r (1-r^2)^{3/4}$$
$$= \frac{\sqrt{2} c_0 (3N)^{3/2}}{7\sqrt{\pi}} \left(\frac{4}{3\pi N}\right)^{1/3} \approx 0.87 N^{7/6}. \tag{A3}$$

The averaged crystallization energy per particle $E_{\rm cr}/N$ is shown in the inset of Fig. 10 by the dashed curve. We see a rather good coincidence of this quantity with the above considered difference of cluster energies per particle of both models shown in the same inset by the solid curve. At least the difference of these two curves (the ratio of the two curves is given in the inset by the dotted line) does not depend on the number of particles.

Next we consider the maximum radius of the cluster which for the discrete model is shown in Fig. 11 by the solid curve. The same quantity for the hydrodynamic model [see Eq. (6)] is shown by the dashed curve. Although both curves

demonstrate the same behavior, they differ quantitatively: the radius calculated in the hydrodynamic model is larger. Such a behavior of the cluster radius is typical for various confinement potentials (see, for instance, Refs. [29,26], where a system of charged particles confined by a Coulomb potential was studied). It is remarkable that the difference of the maximum radii calculated in both models (shown by the dotted line) does not depend on the number of particles in the cluster for a large N and the ratio becomes relatively small for large N.

The physical origin of this discrepancy is related to the same crystallization phenomena and can be explained as follows. Let us assume that the crystallization is just the replacement of the liquid droplet by a regular hexagonal lattice of electrons. If there are N electrons in the dot, then there are $\sqrt{N/3}$ along the radius and $2\sqrt{3N}$ along its perimeter. We also assume that these electrons along the cluster perimeter are made of a thin outer ring of liquid droplets of width h which has the same amount of charge, namely,

$$2\sqrt{3N} = 2\pi \int_{R-h}^{R} rdr\rho_0(r) = 3N \int_{1-h/R}^{1} drr\sqrt{1-r^2} \approx N(h/R)^{3/2}, \tag{A4}$$

which leads to

$$h = \left(\frac{3}{2N}\right)^{1/3}, \quad R = \left(\frac{9\pi}{8}\right)^{1/3} \approx 1.52. \tag{A5}$$

Now if we put these outer particles on a circle with a radius coinciding with the averaged charge position on the above thin ring of the droplet we will obtain the following contraction of the droplet caused by crystallization:

$$\Delta R = \int_{R-h} drr(R-r)\rho_0(r) \Big/ \int_{R-h} drr\rho_0(r) = \frac{3}{5}h = 0.91, \tag{A6}$$

which is in good agreement with the dotted line in Fig. 11.

[1] P. Leiderer, W. Ebner, and V. B. Shikin, Surf. Sci. **113**, 405 (1992).
[2] R. C. Ashoori, Nature (London) **379**, 413 (1996).
[3] J. H. Chu and Lin I, Phys. Rev. Lett. **72**, 4009 (1994).
[4] B. G. Levi, Phys. Today **41**, 17 (1988).
[5] Y. Kondo, J. S. Korhonen, M. Krusius, V. V. Dmitriev, E. V. Thuneberg, and G. E. Volovik, Phys. Rev. Lett. **68**, 3331 (1992).
[6] M. Golosovsky, Y. Saado, and D. Davidov, Phys. Rev. E **65**, 061405 (2002).
[7] M. Saint Jean, C. Even, and C. Guthmann, Europhys. Lett. **55**, 45 (2001).
[8] R. Bubeck, C. Bechinger, S. Neser, and P. Leiderer, Phys. Rev. Lett. **82**, 3364 (1999).
[9] A. M. Mayer, Nature (London) **18**, 258 (1878).
[10] J. J. Thomson, Philos. Mag. **39**, 237 (1904).
[11] B. Partoens and F. M. Peeters, J. Phys.: Condens. Matter **9**, 5383 (1997).
[12] F. Bolton and U. Rössler, Superlattices Microstruct. **13**, 139 (1993).
[13] V. M. Bedanov and F. M. Peeters, Phys. Rev. B **49**, 2667 (1994).
[14] M. Kong, B. Partoens, and F. M. Peeters, Phys. Rev. E **65**, 046602 (2002).
[15] V. A. Schweigert and F. M. Peeters, Phys. Rev. B **51**, 7700 (1995).
[16] A. Melzer, M. Klindworth, and A. Piel, Phys. Rev. Lett. **87**, 115002 (2001).
[17] T. E. Sheridan, Phys. Rev. E **72**, 026405 (2005).
[18] A. Melzer, Phys. Rev. E **67**, 016411 (2003).
[19] Here ω_0 is the unit of frequency, where in Ref. [15] $\omega_0/\sqrt{2}$ was used.
[20] F. M. Peeters, V. A. Schweigert, and V. M. Bedanov, Physica B **212**, 237 (1995).
[21] Y.-J. Lai and L. I, Phys. Rev. E **60**, 4743 (1999).
[22] L. Cândido, J. P. Rino, N. Studart, and F. M. Peeters, J. Phys.: Condens. Matter **10**, 11627 (1998).
[23] L. J. Campbell and R. M. Ziff, Phys. Rev. B **20**, 1886 (1979).
[24] P. Cheung, M. F. Choi, and P. M. Hui, Solid State Commun. **103**, 357 (1997).
[25] B. A. Grzybowski, Xingyu Jiang, H. A. Stone, and G. M. Whitesides, Phys. Rev. E **64**, 011603 (2001).
[26] J. A. Drocco, C. J. Olson Reichhardt, C. Reichhardt, and B. Jankó, **68**, 060401(R) (2003).
[27] Z. L. Ye and E. Zaremba, Phys. Rev. B **50**, 17217 (1994).
[28] L. Bonsall and A. A. Maradudin, Phys. Rev. B **15**, 1959 (1977).
[29] W. P. Ferreira, A. Matulis, G. A. Farias, and F. M. Peeters, Phys. Rev. E **67**, 046601 (2003).